

Nanostructured $\text{Al}_{86}\text{Gd}_6\text{Ni}_6\text{Co}_2$ bulk alloy produced by twist extrusion of amorphous melt-spun ribbons

A.P. Shpak^a, V.N. Varyukhin^b, V.I. Tkatch^{b,*}, V.V. Maslov^a, Y.Y. Beygelzimer^b,
S.G. Synkov^b, V.K. Nosenko^a, S.G. Rassolov^b

^a Institute for Metal Physics of the NAS of Ukraine, 36 Vernadsky St., Kyiv 03142, Ukraine

^b Donetsk Institute of Physics & Engineering of the NAS of Ukraine, 72 R. Luxemburg St., Donetsk 83114, Ukraine

Received 17 November 2005; received in revised form 28 February 2006; accepted 20 March 2006

Abstract

Amorphous $\text{Al}_{86}\text{Gd}_6\text{Ni}_6\text{Co}_2$ ribbons produced by melt-spinning were consolidated using twist extrusion (TE). Transition of the amorphous alloy ribbon into the crystalline state at 5 K/min occurs via three stages in the temperature range from 473 to 673 K. Formation of fcc Al nanocrystals is the dominant process in the first and second stages, which leads to increasing microhardness of ribbons from 360 to 620 kgf/mm². From one to five TE passes were performed on chopped ribbon in several experimental runs at temperatures between 458 and 573 K and applied pressures between 1150 and 1700 MPa. Full consolidation of the ribbons was achieved at TE temperatures ≥ 523 K. The maximum microhardness (550 kgf/mm²) was reached in bulk materials consolidated at 513 K with a nanocomposite microstructure consisting of about 57 vol.% of Al-crystals with a size of about 13 nm embedded in the residual amorphous phase. Extrusion at 573 K resulted in full crystallization of the amorphous phase via precipitation of equilibrium intermetallics and lowering of the microhardness to 380 kgf/mm².

© 2006 Elsevier B.V. All rights reserved.

Keywords: Amorphous Al alloy ribbon; Consolidation; Twist extrusion; Structure; Microhardness

1. Introduction

Amorphous Al-based alloys (≥ 80 at.% Al) containing rare earth (RE) and transition metal (TM) solutes produced by quenching from liquid state possess high ultimate strength (up to 1 GPa), ductility and corrosion resistance [1]. These properties are considerably increased by controlled partial (primary) crystallization resulting in formation of fcc-Al nanocrystals embedded in the residual amorphous matrix [1,2]. The application of high-strength and light-weight Al-based alloys with a nanocomposite microstructure is very promising, and has attracted significant interest of researchers and extensive research work has been done on this class of materials.

Al-based alloys are structural materials, but due to relatively low glass-forming ability (GFA) of alloys investigated up now the maximum size of samples with the fully glassy structure (typically ribbons, flakes or powders) does not exceed several hundreds of micrometers, thus limiting potential applications.

Approaches for solving this problem include the search for alloy compositions in which amorphous phases are formed at low cooling rates in the order of 1–10 K/s (bulk metallic glasses, BMG) as well as production of bulk specimens via consolidation processes in such a way so as to retain the good mechanical properties inherent in amorphous melt-quenched products. One of the main problems of the latter approach is the relatively low thermal stability of Al-RE-TM glasses. Conventional hot extrusion or hot pressing techniques require rather high temperatures (≥ 673 K) [1,3] for full consolidation of Al-based alloys, which does not allow the amorphous and partially crystallized structures with improved mechanical properties to be retained.

On the other hand, recently developed methods of severe plastic deformation [4,5] provide very large strains at relatively low temperatures and are promising for consolidation of rapidly quenched materials with highly nonequilibrium disordered and partially ordered structures. It has been recently established that severe plastic torsion straining at ambient temperature allows nanostructured materials to be produced. Semi-amorphous Al-based powders prepared by mechanical alloying and gas atomization have been compacted [6] as well as amorphous $\text{Ti}_{50}\text{Ni}_{25}\text{Cu}_{25}$ and $\text{Fe}_{82.3}\text{Ni}_{11.8}\text{B}_{5.9}$ alloy ribbons produced by

* Corresponding author. Tel.: +38 62 311 52 89; fax: +38 62 311 52 89.
E-mail address: vit@depm.fti.ac.donetsk.ua (V.I. Tkatch).

melt spinning [7]. The fully consolidated disk-shape samples were 0.2–0.3 mm thick and showed improved physical properties. However, this process does not allow production of large bulk materials.

Equal channel angular extrusion (ECAE) is more convenient for fabrication of bulk samples, and has recently been used to consolidate partially amorphous Al-RE-TM gas-atomized powder at 280 °C [8]. However, full density was not achieved, probably due to the presence of a high volume fraction of brittle intermetallic phases in the as-prepared powder [9]. Detailed analysis of the processes occurring during compaction has shown that almost full consolidation occurred in regions consisting of amorphous and semi-amorphous powder particles at true strains of ~ 2 [9].

It is therefore interesting to further examine severe plastic deformation techniques for consolidation of rapidly quenched Al-based materials with a fully amorphous structure. The relatively new process of twist extrusion (TE) [10,11] may enable fabrication of large cross-section materials, and it was used for the first time in the present study for consolidation of amorphous melt-spun ribbons. The TE method involves passing a billet through a die with a twisted channel (Fig. 1). Cyclic torsional deformation can be applied in subsequent passes, where the torsional strain is applied in either the same direction or the opposite direction relative to the initial torsion. In such a way, the deformation in TE is similar to that in high-pressure torsion processing of thin disks [10,11], where the billet cross-section remains unchanged throughout the extrusion. Although the details are different, ECAE processing similarly allows an accumulation of strain by subsequent extrusion passes.

From a comparison of the ECAE and TE techniques [12] it follows that the latter method has a number of peculiarities in both stress–strain state and technological implementation, which make this process attractive for consolidation of amorphous materials. In particular, the deformation gradient in TE processing is quite steep in the cross-section area and this method is characterized by intense flow of material being deformed within cross-sections of the billet. These factors are very important in

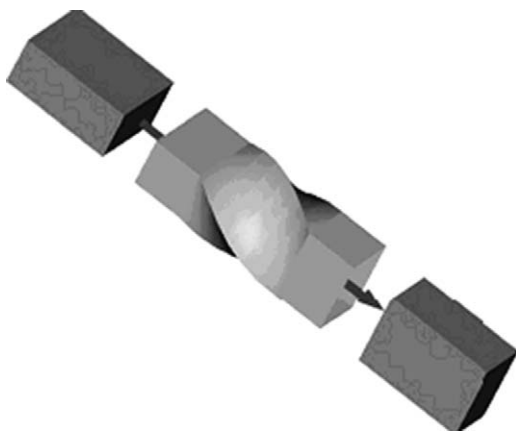


Fig. 1. Schematic illustration showing the principle of twist extrusion (TE) processing, where a sample is passed through a twisted channel. The sample cross-sectional area and shape do not change during this process.

deforming powder materials since they intensify the consolidation processes.

The aim of this paper is to explore the effectiveness of TE in the consolidation of amorphous $\text{Al}_{86}\text{Gd}_6\text{Ni}_6\text{Co}_2$ (atomic percent) alloys produced by melt-spinning [13]. Further, this work examines the influence of TE process parameters on the structure and microhardness of bulk $\text{Al}_{86}\text{Gd}_6\text{Ni}_6\text{Co}_2$ amorphous samples produced by TE.

2. Experimental procedure

Alloy ingots with the nominal composition were obtained by arc melting under purified argon. Elemental Al (99.99%), Ni and Co (99.9%) were used as starting materials, along with an Al_3Gd compound master alloy (Gd 99.7%) that was prepared under similar conditions. The ingots were remelted several times to ensure the homogeneity of the samples. The rapidly quenched ribbons were produced by planar flow casting of the molten alloy heated in a quartz tube to 1223 K and then ejected through a nozzle onto a rotating copper wheel with peripheral speed 25 m/s. Quenching was carried out in an atmosphere of pure helium. The ductile ribbons produced were typically 10–15 mm wide, 40–60 μm thick and up to several meters long. The chemical compositions of the master alloy and melt-spun ribbons were checked by X-ray fluorescence analysis.

For TE consolidation the melt-spun ribbons without preliminary milling were packed into copper cans of 30 mm outside diameter and 100 mm height and cold compacted to about 73% theoretical density. The cans were sealed without prior degassing of the compacted material. The die had a channel with a 15 mm \times 25 mm rectangular cross-section and a twist angle of 60°. The accumulated deformation is 1.2 for each extrusion pass using this die geometry [12]. Prior to extrusion the die and can were heated to the selected extrusion temperature, T_{extr} , and equilibrated for about 15 min. Extrusion was done at a rate of 3 mm/s with back-pressure applied to the exit channel of the die. Since processes similar to mechanical ball milling take place during the first stages of compaction [9], and to improve subsequent consolidation processing, the first extrusion pass was carried out at 423 K—well below the onset crystallization temperature. The can with cold-compacted ribbon changed its cross sectional shape during this extrusion pass, and the cross-section remained unchanged during subsequent passes. From one to five extrusion passes were conducted in several experiments at temperatures from 458 to 573 K and applied pressures in the range of 1150–1700 MPa. The final dimensions of the billets were 14 mm \times 23 mm \times 40 mm.

Structure of the as-prepared and heat treated ribbons as well as of the consolidated samples was characterized by X-ray diffraction (XRD) using an automated DRON-3 M diffractometer with Fe-filtered $\text{Co K}\alpha$ radiation. The thermal stability and results of the phase transformations in amorphous ribbons were monitored under constant rate heating at 5 K/min by electrical resistance measurements using a standard four-probe method. The microstructure of consolidated samples was investigated by light microscopy using a Neophot-32 microscope. Microhardness, H_{μ} , of the melt-spun ribbons and consolidates was

measured using a standard PMT-3 microhardness tester under a load of 0.29 N (30 gf) applied for 10 s. The H_{μ} data reported are the average of 10 indentations and the standard deviation of data does not exceed 2%. The Archimedes method was used for density measurements of the bulk samples.

3. Results and discussion

3.1. Characterization of ribbons

X-ray diffraction showed that the as-quenched melt-spun $\text{Al}_{86}\text{Gd}_6\text{Ni}_6\text{Co}_2$ ribbons were fully amorphous (Fig. 2(a)). Only a broad halo was seen within a wide 2θ range ($30\text{--}60^\circ$), without any trace of sharp peaks related to a periodic lattice structure. The microhardness (H_{μ}) of amorphous ribbons was 360 kgf/mm^2 , which is somewhat higher than for Al–Y–Ni glasses [14] with the same solute content.

A preliminary study of the behavior of melt-spun ribbons under continuous heating was carried out using electrical resistivity to estimate the consolidation temperatures. These measurements (Fig. 3) show that crystallization of amorphous $\text{Al}_{86}\text{Gd}_6\text{Ni}_6\text{Co}_2$ ribbons occurs via three clearly separated reactions. As shown in [15], both the shapes and the temperatures, T_{xi} , of peaks in the dR/dT curves (marked in Fig. 3) coincide with those on the DSC thermogram for $\text{Al}_{85}\text{Y}_8\text{Ni}_5\text{Co}_2$ glass. This indicates that the resistance measurements adequately characterize the crystallization behavior of Al-based glasses. The onset crystallization temperature at 5 K/min was found to be 473 K while all transformations were completed at approximately 700 K. To identify the phases formed in each stage, sample heating was interrupted at temperatures corresponding to the end of each stage. XRD analysis of ribbon heated to 593 K (Fig. 2(b)) shows that the first transformation stage of the amorphous phase is primary crystallization which produces a composite microstructure consisting of Al particles embedded in a surrounding amorphous phase. The (1 1 1) and (2 0 0) Al

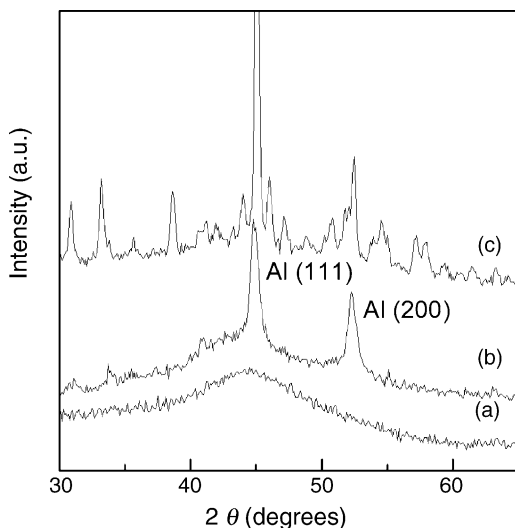


Fig. 2. XRD traces from the as-prepared (a) and heated at 5 K/min up to 620 K (b) and 673 K (c) $\text{Al}_{86}\text{Gd}_6\text{Ni}_6\text{Co}_2$ melt-spun ribbons.

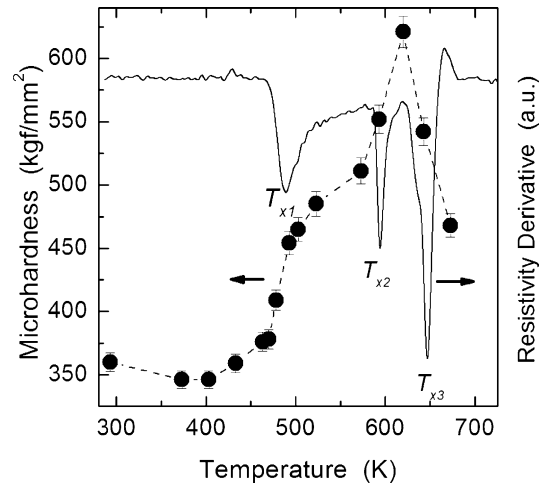


Fig. 3. The rate of resistance changes (dR/dT) upon heating at 5 K/min (right axis) and microhardness (left axis) of the $\text{Al}_{86}\text{Gd}_6\text{Ni}_6\text{Co}_2$ melt-spun ribbons heated to various temperatures.

peaks are very broad indicating the small grain size. The XRD pattern of the sample heated to the end of the second stage (not shown) was quite similar to trace (b) except for several very weak lines and a small bump at left side of the (1 1 1) peak. These XRD results agree well with those reported in [16] for amorphous $\text{Al}_{85}\text{Gd}_8\text{Ni}_7$. Similar to [16] the second transformation stage in the amorphous $\text{Al}_{86}\text{Gd}_6\text{Ni}_6\text{Co}_2$ may be interpreted as local chemical ordering occurring in the residual amorphous matrix and formation of a fine intermetallic phase. The third crystallization step results in disappearance of the amorphous phase and formation of an increased amount of relatively coarse Al phase, together with equilibrium intermetallic phases Al_3Gd , Al_3Ni , Al_9Co_2 and unidentified compound(s) that are probably ternary Al–Ni–Gd intermetallics [16] (Fig. 2(c)).

Microhardness measurements of melt-spun ribbons heated to different temperatures presented in Fig. 3 reveal that structural relaxation occurring below the onset crystallization temperatures slightly decreases the initial value of 360 kgf/mm^2 while the appearance of crystalline phases increases the value of H_{μ} . From Fig. 3, the microhardness changes correspond clearly with the crystallization stages: H_{μ} , sharply increases during the first and second crystallization steps and lowers to 468 kgf/mm^2 during the final stage. Similar microhardness behavior was recently reported for annealed $\text{Al}_{87}\text{Nd}_6\text{Ni}_7$ amorphous ribbons [17]. As seen from Fig. 3 the maximum hardness (as high as 620 kgf/mm^2) is reached in alloys with a mixed microstructure of fine Al particles and intermetallic compounds in a residual amorphous matrix. It must be noted that appearance of crystalline phases resulted in embrittlement of the initially ductile amorphous ribbons.

The breadth of the (1 1 1) and (2 0 0) fcc Al peaks is sufficient to use the well-known Scherrer analysis to estimate the mean Al crystallite particle size, which is about 15–17 nm at the end of the first crystallization stage. The volume fraction of the Al-nanocrystals in the sample was estimated to be about 33% by deconvoluting the amorphous halo and the (1 1 1) and (2 0 0) peaks similar as was done in [18]. This suggests that the number



Fig. 4. A TE-processed billet with dimensions of about 14 mm × 23 mm × 40 mm compacted at 523 K from amorphous $\text{Al}_{86}\text{Gd}_6\text{Ni}_6\text{Co}_2$ melt-spun ribbons.

density of the nanocrystals embedded in the residual amorphous phase is about $8 \times 10^{22} \text{ m}^{-3}$.

3.2. Microstructure and microhardness of consolidated samples

Consolidation of the melt-spun $\text{Al}_{86}\text{Gd}_6\text{Ni}_6\text{Co}_2$ ribbons was performed using TE at 458 K, which is about 20 K lower than the onset crystallization temperature at 5 K/min. This extrusion regime was not sufficient to consolidate the ribbons and only processes of milling the initially long pieces of the ribbons into particles with several millimeter size occurred. XRD of the material produced after one extrusion pass at 458 K showed the presence of a small amount of fcc Al-nanocrystals, showing that severe plastic deformation facilitates crystallization. This is in general accordance with [7], where nanocrystalline phase formation was observed during plastic torsion straining of amorphous $\text{Ti}_{50}\text{Ni}_{25}\text{Cu}_{25}$ ribbons at room temperature.

Experiments performed at higher TE temperatures showed that partial consolidation of the amorphous ribbons takes place at 493–513 K, while fully dense billets were obtained for TE at

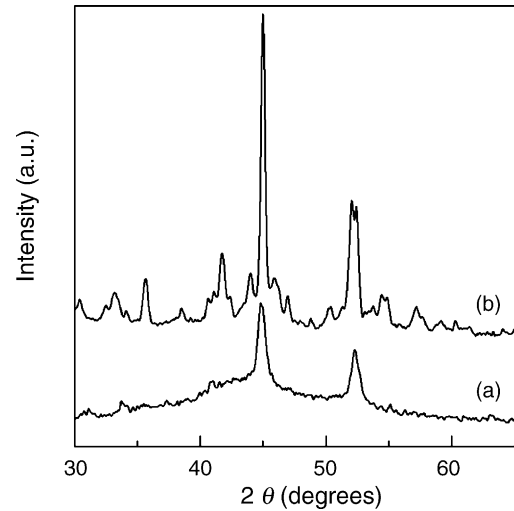


Fig. 6. XRD traces from consolidates produced by TE: (a) at 523 K (three passes) and (b) at 573 K (four passes).

temperatures $\geq 523 \text{ K}$ (Fig. 4). Fig. 5 shows the microstructure of an etched sample consolidated via three TE passes at 523 K. Voids and cracks were practically absent in the structure. Separate ribbons without any structural features at the boundaries may be identified especially in the central part of the billet.

XRD patterns of billets compacted in the range 493–523 K were similar (Fig. 6(a)) and are typical for a nanocomposite structure of Al-nanocrystals embedded in amorphous matrix, which formed in the melt-spun ribbons after the first and second crystallization stages. The XRD pattern from the billet extruded at 573 K (Fig. 6(b)) contains rather narrow peaks of fcc Al together with lines present in the pattern of the fully crystallized ribbon (Fig. 2). These patterns indicate that the phases present after full consolidation via TE at 573 K are similar to those produced by annealing the amorphous ribbon at 673 K.

Analysis of the XRD spectra from consolidates obtained at 493–523 K shows that the sizes of the Al nanocrystals are in the range 12–14 nm and within experimental error are independent of the extrusion temperature. On the other hand, the fraction of crystallized volume present in Fig. 7 depends not only on T_{extr} , but on the number of extrusion passes. For instance, the fraction of crystallized volume formed during five extrusion passes at 513 K (0.57) was appreciably larger than that formed after three passes at 523 K (0.43).

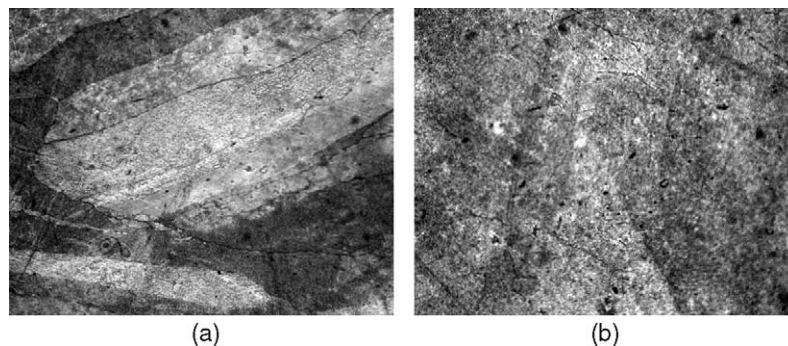


Fig. 5. Optical micrograph of the central (a) and peripheral (b) parts of the three-pass TE billet compacted at 523 K. 1000×.

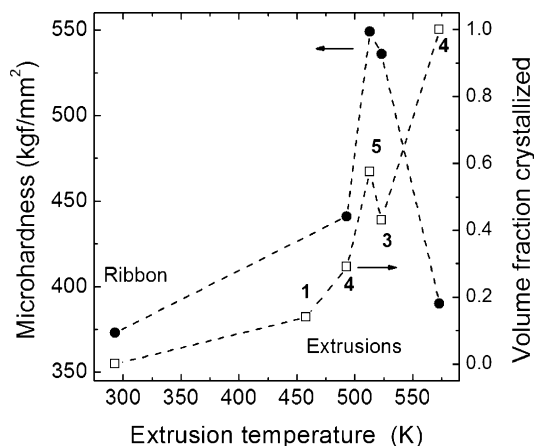


Fig. 7. Microhardness of the amorphous ribbons before and after consolidation (left axis) and the volume fraction crystallized in the compacted samples (right axis) as function of the extrusion temperature. Numbers represent the number of TE passes.

Microhardness of the consolidated samples initially increased with extrusion temperature, exhibited a maximum of 550 kgf/mm^2 at $T_{\text{extr}} = 513 \text{ K}$, and then decreased to 380 kgf/mm^2 (Fig. 7). Comparison of the microhardness measurements and the XRD studies of the consolidated samples suggests that the maximum hardness was reached in bulk materials with a partially crystallized microstructure. This indicates that formation of nanoscale Al crystals in an amorphous matrix during consolidation leads to hardening while crystallization of the equilibrium intermetallics in the residual amorphous matrix as well as coarsening of the Al phase lowers the hardness. The key contribution of the nanocrystalline particles to the hardening is supported by the lower value of H_{μ} of the sample consolidated at 523 K (three passes), which contain 43% of the crystalline phases in comparison with hardness of the sample extruded at 513 K (five passes) with 57% of nanocrystals (Fig. 7).

The microhardness measured on peripheral parts of the billets was up to 10% higher than H_{μ} in the central region. Taking into account the above mentioned differences between structures of the central and peripheral parts of consolidates (Fig. 5) this indicates that the experimental conditions of TE processing do not provide fully homogeneous deformation of the sample [10]. In turn, it may result in inhomogeneity of the nanocrystallization development induced by severe plastic deformation [6] in various parts of the billet. The detailed studies of the possible origin of the observed differences in structure and microhardness in the cross section of the consolidated billets are now in progress.

The maximum microhardness of consolidates (550 kgf/mm^2) is higher than H_{μ} of the as-prepared amorphous ribbon, but lower than the maximum value achieved in the partially crystallized ribbons (Fig. 3). This suggests that the parameters of TE extrusion processing (both extrusion temperature and number of passes) of melt-spun ribbons may require optimization to enhance the microhardness of compacted billets. Nevertheless, the maximum microhardness in TE compacted $\text{Al}_{86}\text{Gd}_6\text{Ni}_6\text{Co}_2$ is higher than the hardness of material obtained by ECAE processing of semi-amorphous $\text{Al}_{85}\text{Y}_{2.5}\text{La}_{2.5}\text{Ni}_{10}$ alloy powder (380 kgf/mm^2) [8].

Despite of the preliminary character of this study, these results suggest that TE processing allows metastable structures formed in rapidly solidified Al-based glassy products to be retained to some extent in bulk product forms. TE may therefore be considered as a promising technique for producing structural materials with improved mechanical properties. It is also expected that further studies, which are in progress will allow development of new high-strength nanostructured Al-based alloys for practical exploitation.

4. Summary

Amorphous $\text{Al}_{86}\text{Gd}_6\text{Ni}_6\text{Co}_2$ produced by melt-spinning crystallizes in three distinct steps in the temperature range from 473 to 673 K under continuous heating at 5 K/min. Formation of fcc Al crystals with sizes between 15 and 17 nm and a volume fraction of about 33% dominate the first and second crystallization stages. Microstructures with these fine Al crystals provide enhancement of the microhardness from 360 to 620 kgf/mm^2 , while appearance of coarse Al particles and intermetallics during the final transformation stage lowers hardness to 468 kgf/mm^2 . Consolidation of amorphous $\text{Al}_{86}\text{Gd}_6\text{Ni}_6\text{Co}_2$ melt-spun ribbons by twist extrusion was performed at 458–575 K and applied pressures of 1150–1700 MPa. Fully dense billets with dimensions of $14 \text{ mm} \times 23 \text{ mm} \times 40 \text{ mm}$ were obtained at temperatures $\geq 523 \text{ K}$, while partial consolidation of the amorphous ribbons occurred at 493–513 K. The maximum microhardness (550 kgf/mm^2) was reached for bulk materials consolidated through five passes at 513 K with a composite microstructure comprised of about 57% of Al-crystals with a size of about 13 nm embedded in a residual amorphous phase. Four-pass TE at 573 K resulted in full crystallization of the amorphous ribbon precursor, lowering the microhardness to 380 kgf/mm^2 . These results demonstrate the potential of TE processing for producing high-strength bulk Al-based alloys with nanocomposite structure from amorphous precursors.

Acknowledgments

The work was partially supported by the National Academy of Science of Ukraine under projects Nos. 38/04-H, 30/05-H and STCU Project No. 2047. Assistance of Dr. V. Krysov in microhardness measurements, Mr. V. Popov in electrical resistance measurements, Mr. A. Synkov in TE compaction is acknowledged. Dr. D. Miracle is acknowledged for a critical reading of the manuscript.

References

- [1] A. Inoue, *Progr. Mater. Sci.* 43 (1998) 365–520.
- [2] G.S. Choi, Y.H. Kim, H.K. Cho, A. Inoue, T. Masumoto, *Scr. Metall. Mater.* 33 (8) (1995) 1301–1306.
- [3] A. Inoue, H. Kimura, *Mater. Sci. Eng. A* 286 (2000) 1–10.
- [4] R.Z. Valiev, R.K. Islamgaliev, I.V. Alexandrov, *Progr. Mater. Sci.* 45 (2000) 103–189.
- [5] Y.T. Zhu, T.C. Lowe, T.G. Langdon, *Scr. Mater.* 51 (2004) 825–830.
- [6] W.J. Botta Filho, J.B. Fogagnolo, C.A.D. Rodrigues, C.S. Kiminami, C. Bolfarini, A.R. Yavari, *Mater. Sci. Eng. A* 375–377 (2004) 936–941.

- [7] R.Z. Valiev, V.G. Pushin, D.V. Gunderov, A.G. Popov, *Dokl. Akad. Nauk* 398 (2004) 54–59 (In Russian).
- [8] O.N. Senkov, D.B. Miracle, J.M. Scott, S.V. Senkova, *J. Alloys Compd.* 365 (2004) 126–133.
- [9] O.N. Senkov, S.V. Senkova, J.M. Scott, D.B. Miracle, *Mater. Sci. Eng. A* 393 (2005) 12–21.
- [10] Y. Beygelzimer, D. Orlov, V. Varyukhin, in: Y.T. Zhu, T.G. Langdon, R.S. Mishra, S.L. Semiatin, M.J. Saran, T.C. Lowe (Eds.), *Ultrafine Grained Materials II*, TMS, 2002, pp. 297–304.
- [11] V.V. Stolyarov, Y.E. Beygelzimer, D.V. Orlov, R.Z. Valiev, *Phys. Met. Metallogr.* 99 (2) (2005) 204–211.
- [12] Y. Beygelzimer, *Mech. Mater.* 37 (2005) 753–767.
- [13] V.V. Maslov, V.K. Nosenko, V.A. Mashira, V.I. Tkatch, S.G. Rassolov, V.V. Popov, V.I. Krysov, *Metallofys. Novejsh. Technol. (Met. Phys. Adv. Tech.)* 27 (7) (2005) 937–948 (in Russian).
- [14] H.S. Kim, *Mater. Sci. Eng. A* 304–306 (2001) 327–331.
- [15] J.O. Wang, H.W. Zhang, X.J. Gu, K. Lu, F. Sommer, E.J. Mittemeijer, *Mater. Sci. Eng. A* 375–377 (2004) 980–984.
- [16] M.C. Gao, G.J. Shiflet, *Intermetallics* 10 (2002) 1131–1139.
- [17] P. Rizzi, R. Doglione, L. Battezzati, *Mater. Sci. Eng. A* 375–377 (2004) 969–974.
- [18] J.S. Blazquez, V. Franco, C.F. Conde, A. Conde, *JMMM* 254/255 (2003) 460–462.